LUT University

Modelling of indirect steam gasification in circulating fluidized bed reactors

Myöhänen Kari, Palonen Juha, Hyppänen Timo

Modelling of indirect steam gasification in circulating fluidized bed reactors

Kari Myöhänen[1*], Juha Palonen[2], Timo Hyppänen[1]

[1]*Lappeenranta University of Technology, FI-53850 Lappeenranta, Finland*

[2]*Sumitomo SHI FW Energia Oy, FI-78200 Varkaus, Finland*

*Email: *kari.myohanen@lut.fi*

Abstract

The indirect steam gasification in circulating fluidized bed reactors was studied by modelling. The object of study was a coupled 12 MW_{th} gasifier-combustor system, which was fired by woody biomass. The heat for the steam-blown gasifier was produced in the air-blown combustor and transported by circulating solids between the interconnected reactors. The system was modelled by a semi-empirical three-dimensional model, which simulated the fluid dynamics, reactions, and heat transfer in the coupled process. The studied cases included different temperature levels, which were controlled by the amount of additional fuel feed to the combustor. The model concept can be later applied to study sorption enhanced gasification, which is a promising method for sustainable production of transport fuels to substitute fossil based fuels.

Keywords: allothermal gasification; semi-empirical model; dual fluidized bed; biomass gasifier

1.   Introduction

Gasification of biomass is a method to produce renewable, carbon neutral energy, which, unlike wind and solar, is not dependent on weather conditions. The gasification generates producer gas, which contains high share of combustible gas components: carbon monoxide, hydrogen, and hydrocarbons. The producer gas can be combusted for producing heat and electricity, but it can also be converted to different products, such as synthetic natural gas (SNG), Fischer–Tropsch diesel, dimethyl ether (DME), and methanol.

The terms "producer gas" and "syngas" are often mixed. Producer gas (or product gas) is simply the gas exiting the gasifier. Depending on the gasification technology and process conditions, the composition of the producer gas can vary largely: in addition to above mentioned combustible gases, it can contain large amounts of carbon dioxide, water vapour, and nitrogen. Syngas (synthesis gas) is a gas for chemical synthesis and it mainly consists of carbon monoxide and hydrogen. Conversion of producer gas to syngas involves e.g. catalytic cracking of tars, reforming of hydrocarbons, filtration, and possible modification of the CO/H_2-ratio by shift conversion. This article focuses on the gasification process and the gas from gasifier is referred to as producer gas.

The gasification technologies are categorized to direct (autothermal) gasification and indirect (allothermal) gasification. In direct gasification, the fuel is partially oxidized to generate heat to sustain the gasification process. This can be accomplished by air-blown or steam/oxygen-blown methods. The disadvantage of air-blown method is the high amount of nitrogen in the producer gas, which decreases the heat value of the gas. This is avoided in steam/oxygen-blown method, but this is expensive due to need for air separation unit to produce oxygen. In indirect gasification, the heat for gasification is imported from outside the gasifier reactor. This can be accomplished by heat exchangers, but this is thermally inefficient and technologically difficult due to high temperature requirements. Another method is to apply circulating hot solids as heat carriers, which is the object of this study.

Fig. 1 presents the basic principle of indirect steam gasification of biomass. The total process consists of two interconnected reactors: a gasifier and a combustor. The hot bed material, which consists of fuel ash, make-up sand, and sorbent, is transported from air-blown combustor to gasifier, where it provides heat for the gasification reactions. The producer gas from the steam-blown gasifier is free from atmospheric nitrogen and mainly consists of combustible gases (CO, H_2, C_xH_y), water vapour, and carbon dioxide. The cold bed material

from the gasifier is transported back to combustor to be re-heated. The remaining unreacted char in the circulating solids is combusted in the combustor. Depending on the desired conditions, this can be the only fuel source for the combustor, or additional fuel can be fed to combustor to increase the temperature level of the process.
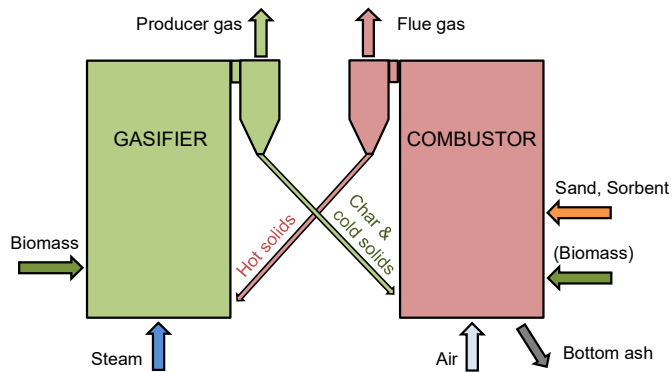

Fig. 1. Basic principle of indirect steam gasification of biomass.

Various concepts have been proposed for indirect steam gasification by using fluidized bed technology [1]. For example, each reactor can be designed for bubbling fluidized bed (BFB) or circulating fluidized bed (CFB) mode and the coupling arrangements can be different. However, the general principle in all of them is similar to above description and commonly these concepts can be called as dual fluidized bed (DFB) gasifiers. The following reviews briefly the development of DFB processes and their recent status.

In 1970's a Pyrox process was developed in Japan by Kunii and co-workers [2]. Interestingly, a similar concept was patented in United States in 1974 [3]. The Pyrox process was targeted for gasification of solid waste materials and it was using a similar principle as the Kunii-Kunugi process, which was for thermal cracking of heavy hydrocarbons [4]. A demonstration plant was constructed in 1976 near a paper and pulp plant in Miyagi Prefecture [2]. The system consisted of two fluidized bed reactors: a cracking reactor (gasifier) and a regenerator (combustor). The process was similar to one shown in Fig. 1, but instead of cyclones, the circulating solids were separated in updraft chambers with larger diameter and smaller fluidization velocity compared with the lower sections of the reactors. The feedstock included organic sludge, waste plastics, municipal solid waste (MSW), and tires. A commercial scale Pyrox unit with a capacity of 450 t/d MSW was built to Funabashi City in 1983 and operated for 8 years [1,5]. Recently, West Biofuels has commissioned a pilot-scale Pyrox unit in Woodland, California [6]. The pilot uses wood pellets with a capacity of 5 t/d, which equals thermal input of about 1 MW_{th}.

The SilvaGas process was invented by Battelle in the early 1980's [7]. In the SilvaGas process, both reactors operate in circulating fluidized bed (CFB) mode, i.e. according to Fig. 1. The rights were later purchased by FERCO (Future Energy Research Corporation) and the process was demonstrated at commercial scale in Burlington, Vermont [7]. The plant was successfully operated from 1997 to 2001 using wood chips and pellets as fuel up to 350 t/d [8]. In 2009, the SilvaGas process was acquired by Rentech [9]. Demonstration scale tests were carried out in Natchez, Mississippi and Commerce City, Colorado, but these plants have now been closed down due to economical reasons [10].

Technical University of Vienna developed a FICFB gasifier in late 1990's [11]. In the FICFB (fast internally circulating fluidized bed) process, the gasifier is operated in bubbling bed mode and the combustor in CFB mode. In 2002, an 8 MW_{th} biomass CHP (combined heat and power) plant using the FICFB concept was commissioned in Güssing, Austria [12]. Since then, several commercial FICFB units have been built and started operation, e.g. 15 MW_{th} unit in Villach, Austria (2010), 14 MW_{th} unit in Senden/Ulm, Germany (2012), and 32 MW_{th} unit in Gothenburg, Sweden (2015) [13,14].

In the MILENA process, the gasifier is operated in CFB mode and it is surrounded by a BFB combustor. A lab-scale MILENA gasifier was built in 2004 by ECN (Energy research Centre of the Netherlands) followed by an 800 kW_{th} pilot unit in 2008 [15]. In 2014, Royal Dahlman started construction of a 4 MWth MILENA gasifier for Ruchi Soya crushing plant at Washim, India[16]. In recent years, plans and engineering studies for larger scale (e.g. 12 MWth) demonstration units have been done [17,18].

The performance of gasifiers can be improved by using catalytic bed materials, which enhances the reforming reactions of tar and methane and thus reduces the amount of tar and increases the amount of

hydrogen in the producer gas. Various artificial catalysts have been tested, many of them nickel-based metal oxides [19,20]. For example, using a Ni-catalyst 20 wt-% of bed material in a 100 kW$_{th}$ DFB pilot, the H_2/CH_4 ratio increased from 3 to above 6 and the tar content decreased from 2.1 to 1.4 g/m^{3}n,dry [21,22]. Natural catalysts, such as olivine, bauxite, and ilmenite, are less effective, however, they are less toxic and cheaper, thus a better choice for commercial operations [12,23–26]. As an example, in Güssing DFB, using olivine instead of quartz sand, the tar content in producer gas was approximately halved [12].

Using CaO containing bed material in gasifier and adjusting the reactor temperatures such that the gasifier operates below and the combustor above the calcination temperature allows transport of CO_2 from the gasifier to combustor [27–29]. The CO_2 is captured in the gasifier by carbonation and released in the combustor due to calcination. This method is called as absorption enhanced reforming (AER) [30], sorption (or sorbent) enhanced gasification (SEG) [31], or even CaO based chemical looping gasification [32]. If the combustor is oxygen-fired, then it is possible to integrate the process with carbon capture and storage (bio-CCS), but so far this concept has not been demonstrated.

In AER/SEG process, decreasing the CO_2 in the gasifier increases the share of other gases, e.g. H_2, CO, and hydrocarbons. Moreover, lower CO_2 concentration promotes the shift conversion reaction and steam reforming of methane, thus increases the amount of H_2 even further. The lower operating temperature of the gasifier reduces the reaction rates, but this is at least partly compensated by longer residence time of solids due to lower bed material circulation between the reactors [33]. Using this technique, the H_2 content in a DFB pilot plant could be increased from about 40 %-vol,dry up to 75 %-vol,dry [34]. In Güssing DFB, the H_2 content was increased to 51 %-vol,dry compared with about 40 %-vol,dry in standard operating mode [33,35]. At the same time, the tar content reduced from 2 – 5 g/m^{3}n,dry to about 1 g/m^{3}n,dry indicating catalytic effects of the limestone based bed material. In a Horizon 2020 project FLEDGED (FLExible Dimethyl ether production from biomass Gasification with sorption-enhancED processes), the sorption enhanced gasification is applied to produce tailored syngas, which has an optimal composition for dimethyl ether synthesis [36]. The physical properties of DME are similar to liquefied petroleum gas (propane, butane) and it can be applied as a substitute for diesel fuel [37,38].

The modelling of indirect steam gasification process has been usually carried out using a flowsheet software, such as Aspen Plus, IPSEpro, Belsim-Vali, or Matlab/Simulink. The simulation of the gasification process can be based on:

- thermodynamic equilibrium [39,40],
- restricted thermodynamic equilibrium [6,41],
- kinetic mechanism [42,43], or
- experimental data [44,45].

An alternative simulation method is to apply neural network modelling [46]. However, this approach relies on extensive experimental data, which is often not readily available.

As the reactions in the gasifier (e.g. shift conversion) progress along the reactor and are affected by local process conditions (e.g. gas composition and temperature), a more detailed description of the process can be achieved by discretizing the reactor model to blocks along the height of the reactor. These approaches are called as one-dimensional (1D) models [47–49]. If the riser of the circulating bed is modelled with core-annulus approach, the model may be referred to as a 1.5D-model [50], but this terminology is not always followed. For simulation of the reactions, these models apply kinetic rate expressions, which are derived from literature, but sometimes adjusted based on available empirical data.

For more detailed analysis, the reactor can be modelled three-dimensionally. Until quite recently, the only 3D modelling of fluidized bed gasifiers were given by Petersen and Werther [51] and our research group [52,53]. The model by Petersen and Werther adopted unsteady state and isothermal conditions, while our model applies steady state and includes solving of heat transfer and temperature fields. The benefit of three-dimensional modelling is that it can simulate the lateral mixing and distribution of different reactants. The lateral mixing of different reacting solids and gases is slower than vertical convection, which leads to uneven distribution of reactants, which may have large effects on process performance especially in large reactors.

Recently, Multi-Phase Particle-In-Cell (MP-PIC) approach has been applied for simulating indirect steam gasification. In this approach, the gas phase is treated as a continuum (Eulerian frame) and the solid phase is treated as particles grouped to parcels (Lagrangian frame) [54,55]. Liu et al . [56] present a simulation

of a pilot-scale DFB and Kraft et al. [57] present a simulation of Güssing DFB, both using Barracuda software. Yan et al. [58] performed a simulation of a small scale DFB applying OpenFOAM, which is a license-free software. The MP-PIC approach uses transient simulation, the typical simulation times are in the order of 100 – 150 seconds, which requires calculation times in the order of 1 – 2 weeks using GPU accelerated computation [56,57]. Due to high computational cost, the MP-PIC models are often simplified, e.g. omitting gasification reactions of char [57], formation of tar [56–58], sorbent reactions [56–58], and using isothermal conditions [58].

This paper presents a modelling method, which is suitable for simulating interconnected fluidized bed processes. The reactors are modelled three-dimensionally using the earlier developed semi-empirical modelling concept [52]. The model approach is comprehensive: it combines modelling of all major heterogeneous and homogeneous combustion and gasification reactions, fluid dynamics of gas and solids, and heat transfer. The novelty in this study is that the gasifier and combustor reactors are interconnected in the model, thus providing a full-loop simulation of the complete DFB system. Compared with fundamentals-oriented CFD models, the calculation time is small, in the order of few hours with a normal desktop PC, thus enabling practical engineering studies. This method was applied to study the effect of different gasification temperatures on the producer gas composition, heat value of gas, and cold gas efficiency. The object of study was a coupled gasifier-combustor system, in which both reactors were operated in CFB mode. The temperature level was adjusted by changing the fuel feed to combustor while keeping the fuel feed to gasifier at a constant value.

2.   Modelling method

The coupled CFB reactors were simulated by a semi-empirical, steady-state engineering model [52,59]. The model combines fundamental balance equations with empirical correlation models and solves the process variables in a three-dimensional domain, which is discretized by a Cartesian structural mesh. The model solves fluid dynamics of gas and solids, combustion and gasification reactions, limestone reactions, attrition of solids, and heat transfer within the suspension and to heat transfer walls. The validation of the model is based on measurements ranging from pilot-scale to commercial-scale combustor and gasifier units [53,60]. Fig. 2 illustrates the modelled reaction paths for fuel conversion in a CFB.
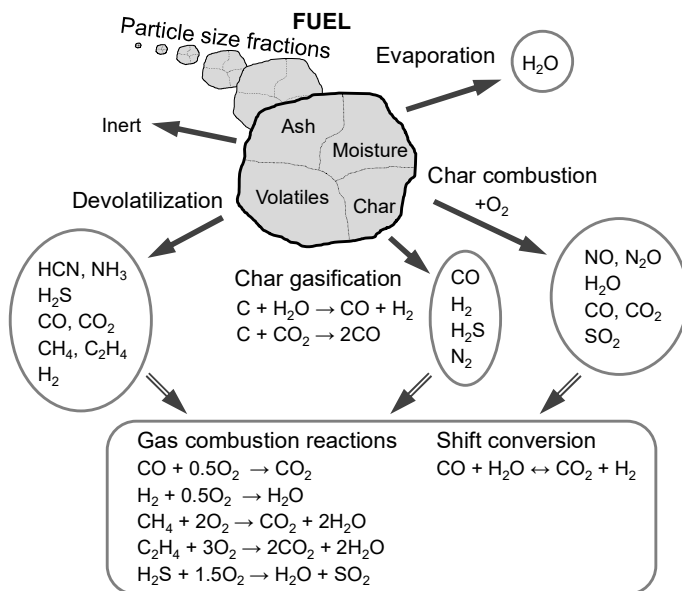

Fig. 2. Modelled reaction paths.

In the 3D model frame, the gasifier and combustor were directly coupled, i.e. the circulating solids separated in the cyclone of one reactor were applied as the incoming circulating material for the other reactor. The solid concentration fields inside the reactors are set based on empirical correlations [52]. Alternatively, the 3D solid concentration data could be set by externally solved CFD results [61], but this was not applied in this study. Usually, in CFB combustor studies using this model, the solids are discretized to six particle size groups and the comminution rate of each size fraction is set based on measured particle size distributions of

different feeds and ash outputs. In this case, the comminution was not solved and the bed phase consisted of one size fraction with particle size 153 µm. By fixing the solid concentration field, the net solids velocity field can be solved by potential flow approach. For solving the internal circulation of solids, which occurs due to downflow of particles at the walls, a superimposed wall layer model is applied. At each calculation cell, which resides by a vertical wall, part of the solids flows to a wall layer cell, where the solids are accumulated and flow downwards until the wall ends. In addition, some of the solids are backmixing from wall layer cell back to main calculation cell near the wall. The solid mass flow entering the wall layer and the back mixing are proportional to local solid concentration. The pressure field is solved by combining a continuity equation of gas and a simplified momentum equations, in which the force due to pressure gradient is equal to interphase force between solids and gas determined by a macroscopic drag term. The gas velocity field is then solved from the pressure field. The convective flow of fuel is solved by solving the momentum balance of fuel inertia, gravity, and drag force from gas and solids [62]. Thus, the concentration field of combustible fuel is not empirically set but solved by the continuity and momentum equations. The mixing of different solid and gaseous species is controlled by diffusion in analogy to Fick's law.

The reaction paths illustrated in Fig. 2 include all the major combustion and gasification reactions, which are encountered in a coupled gasifier-combustor system. The distribution of fuel to ash, moisture, volatiles, and char (fixed carbon) is usually determined by a standard proximate analysis [63]. As the fuel enters the gasifier, the moisture is evaporated and the volatile components released due to presence of hot circulating solids and gas. The carbon in char reacts with water vapour and carbon dioxide in gasification reactions: water-gas reaction (Eq. (1)) and Boudouard reaction (Eq. (2)):

$$C(s) + H_2O(g) \rightarrow CO(g) + H_2(g) \tag{1}$$
$$C(s) + CO_2(g) \rightarrow 2CO(g) \tag{2}$$

Any unreacted char, which is circulated to combustor, is burned in presence of oxygen. With biomass, the share of volatiles is high and the devolatilization process mostly determines the composition of gas in the gasifier. With zero oxygen, the homogeneous oxidation reactions are prevented and only the reversible shift conversion affects the gas composition in the gasifier:

$$CO(g) + H_2O(g) \leftrightarrow CO_2(g) + H_2(g) \tag{3}$$

The total elemental composition of the burning fuel, i.e. char and volatiles, is determined by ultimate analysis [63]. This defines the amount of carbon (C), hydrogen (H), nitrogen (N), sulphur (S), and oxygen (O) in dry, ash-free fuel. In more simplified combustion models, the char is assumed to consist of carbon only and the composition of volatiles can be calculated from the balance (e.g. [57,64,65]). For most solid fuels, the share of carbon in char is over 90%, thus, in terms of heat generation and composition of major gases this approach would not cause a large error. However, for more accurate modelling of formation of sulphur and nitrogen emissions, this would be false as these components are found both in char and volatiles [63]. In this model, the distributions of different elements (C,H,N,S,O) to char and volatiles are specified as input values. The data can be based on bench scale studies or defined by correlations, which have been determined in laboratory scale studies of different fuels. In real furnaces, the distribution may be slightly different from laboratory conditions. For example, the devolatilization is affected by the surrounding temperature and gas atmosphere, heating rate of the particle, particle shape and size and the internal structure of the particle [66,67]. Moreover, the real devolatilization process is transient: the lighter hydrocarbons are released faster than the heavy hydrocarbons. These phenomena are neglected in order to keep the model simple to enable practical calculation of full scale processes.

The reaction rates for evaporation (Eq. (4)), devolatilization (Eq. (5)), and char combustion (Eq. (6)) are determined by empirical correlations, the forms of which are given below:

$$R'''_{wat,i} = a_{wat} \left(\frac{d_{p,i}}{d_{ref}}\right)^{b_{wat}} \exp\left(\frac{-E_{wat}}{RT}\right) \varepsilon_{wat,i}\rho_{wat} \tag{4}$$

$$R'''_{vol,i} = a_{vol} \left(\frac{d_{p,i}}{d_{ref}}\right)^{b_{vol}} (1 - w_{H2O,i})^{c_{vol}} \exp\left(\frac{-E_{vol}}{RT}\right) \varepsilon_{vol,i}\rho_{vol} \tag{5}$$

$$R'''_{char,i} = a_{char} \left(\frac{d_{p,i}}{d_{ref}}\right)^{b_{char}} C_{O_2}^{c_{char}} \exp\left(\frac{-E_{char}}{RT}\right) \varepsilon_{char,i}\rho_{char} \tag{6}$$

The water-gas and Boudouard reaction rates are defined by the following equations, which are simplified forms of the expressions used by Petersen and Werther [50]:

$$r'''_{watg,i} = 235.3 \, C_{C,i}C_{H_2O} \exp\left(\frac{-15\,500}{T}\right) \tag{7}$$

$$r'''_{boud,i} = 7.696 \cdot 10^6 \, C_{C,i}C_{CO_2} \exp\left(\frac{-30\,600}{T}\right) \tag{8}$$

The reaction rate of the shift conversion is defined by Eq. (9), which is based on literature [68,69], but corrected by a multiplier 0.1 according to Petersen and Werther [50] .

$$r'''_{shift} = 0.278 \exp\left(\frac{-1515.46}{T}\right)\left[C_{CO}C_{H_2O} - \frac{C_{CO_2}C_{H_2}}{0.0265 \exp\left(\frac{3956}{T}\right)}\right] \tag{9}$$

A positive value of r'''_{shift} means that the direction of the shift conversion is towards right, e.g. increasing the share of hydrogen in producer gas. A negative value means direction towards left, e.g. increasing the share of carbon monoxide. In steam-blown gasification, the concentration of water vapour is high, thus, usually, the direction is towards right.

The current model does not simulate the formation of tars. The tars are complex heavy hydrocarbons, e.g. levoglucosan and naphthalene, which are formed during gasification and can cause fouling of the downstream equipment. In steam-blown gasification, the measured amount of tar in producer gas has been in the order of 2...5 g/m³n,dry [34,35]. This is equivalent to less than 0.1 mol-% share in the producer gas, thus, it has relatively small impact on the producer gas composition.

3. Model setup

Fig. 3a presents the modelled reactor system. The diameters of the gasifier and combustor were 1.6 m and 1.4 m respectively. The height of the reactors was 15 m. The solids separated by the cyclone of the gasifier were returned to combustor at height 0.3 m. The solids from combustor were returned to gasifier at height 0.5 m. The gasifier was fluidized by steam through the bottom of the reactor. Secondary steam flow was introduced at height 1.9 m together with the fuel feed. The combustor was fluidized by primary air through the grid. Secondary air was fed at height 1.1 m together with make-up sand and limestone. Additional fuel was fed to combustor at height 0.5 m.

Fig. 3b presents the model mesh for gasifier (left) and combustor (right). The dimensions of hexahedral calculation cells were 0.145...0.200 m. The number of cells was about 6300 for gasifier and about 3800 for combustor. With a coarse mesh, the calculation with the semi-empirical model is fast. The calculation time for all cases was in the order of few hours with a normal laptop computer. Some additional time was spent for adjusting the air flow rates so that the excess oxygen (in dry basis) was the same in all cases. The mesh

independency was not checked, but based on earlier studies, the semi-empirical model is not sensitive to mesh density [62]. Besides, the earlier model validations have been performed using coarse meshes.

Fig. 3 a) Reactor system b) Mesh.

The applied fuel was woody biomass (Table 1). Additional solid feeds included inert make-up sand and limestone, which was set to be 100% CaCO$_3$. The boundary conditions are given in Table 2. In the basic case (A01), the fuel feed to combustor was set to 0.1 kg/s, which produced typical operating temperatures for steam blown DFB gasifier: almost 800°C in the gasifier and about 880°C in the combustor. In Case A02, the fuel feed was increased by 50%, which increased the temperature levels by 40°C, but still keeping the maximum temperature in the system below 950°C, which should be safe in terms of agglomeration. In Case A03, the fuel feed was decreased 50% from the basic case. In Case A04, the fuel feed to combustor was zero, thus, all the heat for the system originated from combustion of unreacted char, which flowed from gasifier to combustor. The purpose of the last case was to determine, whether it is possible to operate the gasification process without any additional fuel feed to combustor. The fuel feed and the air flow feed to combustor were the only variable parameters. The air flow rate to combustor was adjusted so that the oxygen concentration after the combustor was 3.94 vol-%,dry. The limestone feed was small, thus, the calcination and carbonation reactions were not affecting much on the gas compositions. The thermal boundary of the walls was set by specifying the walls as refractory lined with thickness of 0.1 m, thermal conductivity 0.5 W/mK, and outer shell temperature 100°C, i.e. assuming that the reactors are well insulated, but with a small heat loss through all walls.

Table 1. Fuel properties.

Proximate analysis, as fired (w-%)		Ultimate analysis, dry, ash-free (w-%)	
Fixed carbon	11.1	Carbon	51.0
Volatiles	61.7	Hydrogen	6.1
Moisture	25.0	Nitrogen	0.5
Ash	2.2	Sulphur	0.1
		Oxygen	42.3
Heat value (MJ/kg)			
HHV, dry solids	20.51		
LHV, as fired	13.76		

Table 2. Boundary conditions.

Parameter	Units	Case A01	Case A02	Case A03	Case A04
Steam flow to gasifier	(kg/s)	0.45	...	...	...
Primary steam ratio	(%)	40	...	...	...
Steam temperature	(°C)	180	...	...	...
Air flow to combustor	(kg/s)	1.84	2.06	1.62	1.38
Primary air ratio	(%)	50	...	...	...
Air temperature	(°C)	280	...	...	...
Fuel feed to gasifier	(kg/s)	0.9	...	...	...
Fuel feed to combustor	(kg/s)	0.10	0.15	0.05	0.00
Sand feed to combustor	(kg/s	0.05	...	...	...
Limestone feed to combustor	(kg/s)	0.01	...	...	...
Solid feed temperatures	(°C)	30	...	...	...

4.   Model results

Fig. 4 presents the modelled temperature and concentrations of oxygen, carbon monoxide and hydrogen at outer surfaces of the reactors of basic case (0.1 kg/s fuel feed to combustor). Fig. 5 presents the same data for the centre-planes of the reactors. In each image, the gasifier is located on left and combustor on right. The profiles were looking fairly similar in all cases, thus, only the basic case is presented as contour plots while line graphs are used for comparing the results of different cases.
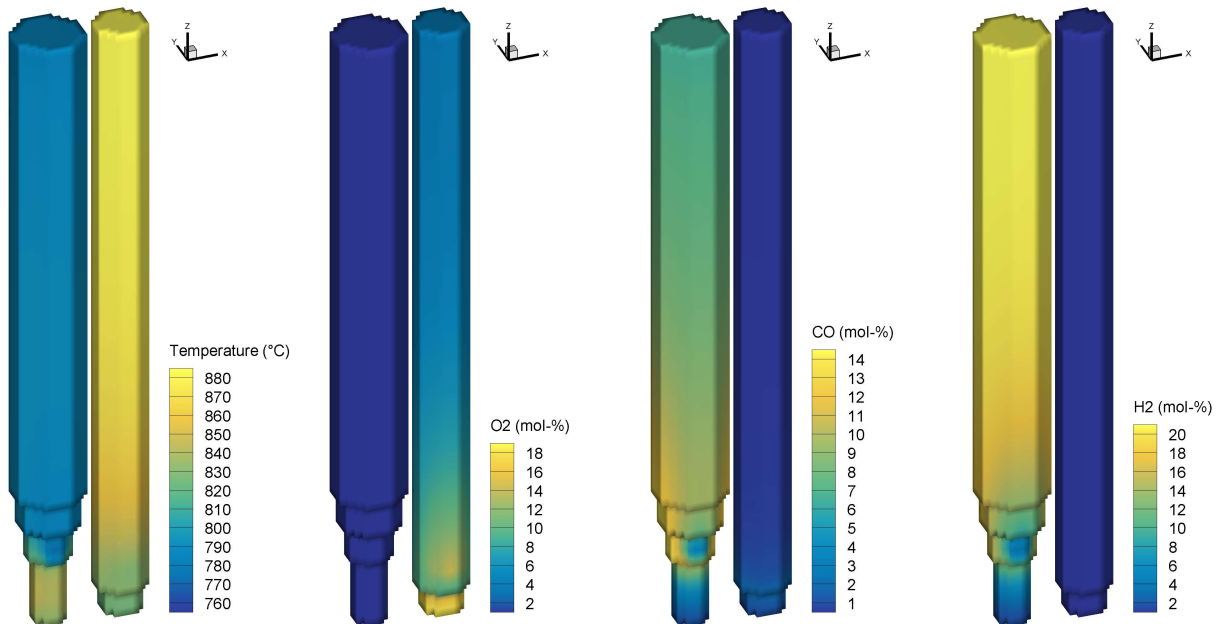

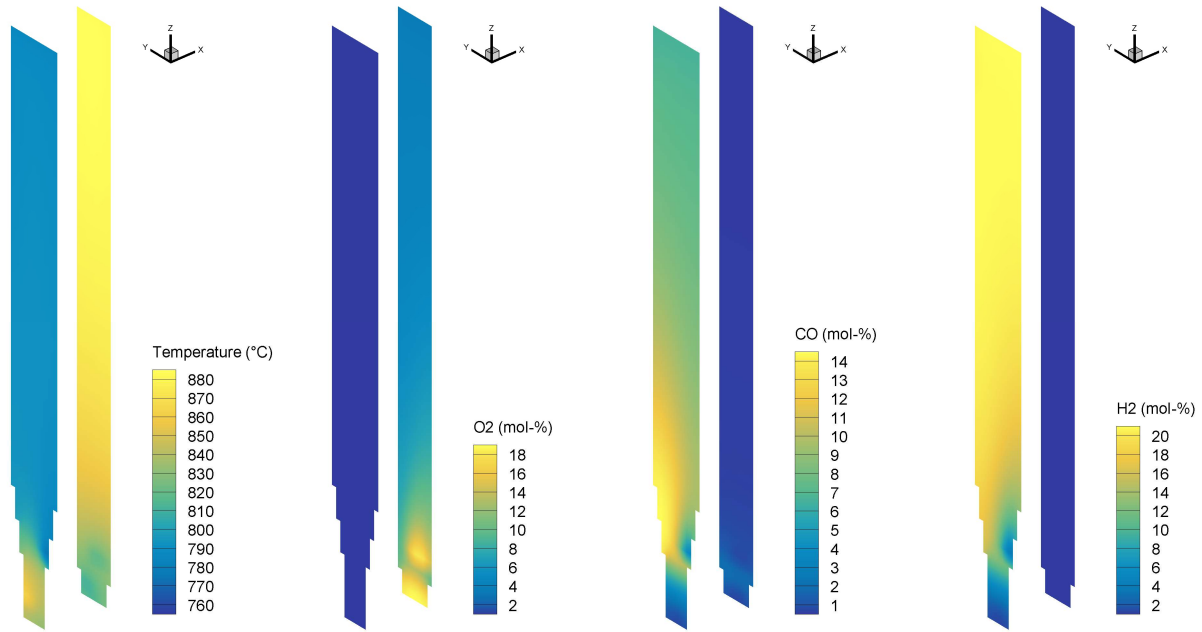Fig. 4. Modelled 3D fields of basic case at outer surface of reactors.

Fig. 5. Modelled 3D fields of basic case at centre-plane of reactors.

In the combustor, most of the fuel burns at the lower section of the furnace and consumes the oxygen, which originates from the primary and secondary air feeds. Some local CO and H_2 is found in the combustor near the fuel inlet, but the concentrations are very small. The combustion reactions heat up the circulating solids in the combustor. The hot solids from the combustor are transferred to lower section of the gasifier, where a locally higher temperature zone is formed. At the location of the fuel feed to gasifier, the temperature decreases rapidly, mostly due to evaporation of fuel moisture. In the gasifier, the combustible gases, such as CO and H_2, originate from devolatilization and water-gas reaction. In the upper section of the gasifier, the CO content decreases and the H_2 content increases due to shift conversion. Based on the model results, the lateral mixing of solid and gaseous species needs to be considered near the fuel and air inlets and return legs, but at the upper sections, the lateral profiles are fairly uniform.

Fig. 6 presents the vertical gas concentration profiles in the centre-line of the gasifier for the basic case. The composition of combustible gases is mainly affected by devolatilization, water-gas reaction, and shift conversion, which are shown in Fig. 7. As seen in Fig. 7, a relatively large devolatilization rate is found at the bottom of the reactor, below the fuel feeding point. This is because the devolatilization is not instantaneous, but governed by Eq. (5). Depending on the fuel properties, such as particle size, density, and moisture, some of the fuel has time to flow to the bottom of the reactor before complete devolatilization. Naturally, the devolatilization rate is highest at the location of the fuel feed. Because steam is used as fluidization gas, the concentration of water vapour is nearly 100% at the bottom of the gasifier. A local peak in the H_2O-profile can be seen at the level of the fuel feed, which is due to evaporation of fuel moisture. In the lower section, the share of H_2O decreases rapidly due to dilution by other gas sources: devolatilization and gasification of char. With biomass, the share of volatiles is high, thus, the source of CO from gasification of char (water-gas reaction) is much smaller than the source of CO from volatiles. In this case, the production of CO and H_2 from volatiles was about identical in molar basis. At the upper section of the gasifier, the H_2 and CO_2 concentrations are increasing while H_2O and CO concentrations are decreasing. This is due to shift conversion, which is highest just above the fuel feed and then continues throughout the gasifier. The shift conversion rate decreases towards the top of the gasifier due to decreasing share of reactants (H_2O and CO). Just before the roof, the water-gas reaction rate drops rapidly. This is due to char flowing to the entrance of the cyclone thus reducing the amount of reactant in that zone.
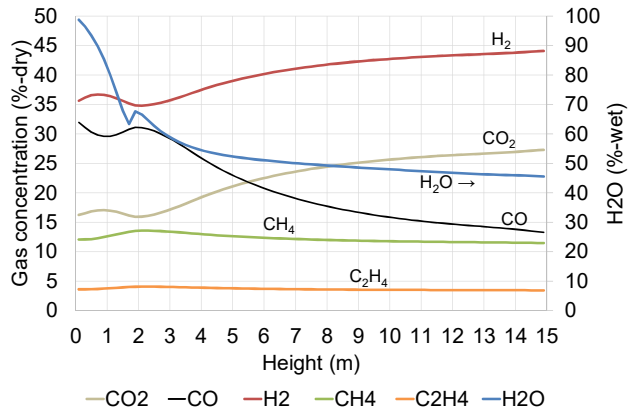
Fig. 6. Gas concentration profiles in the centre-line of the gasifier for basic case.
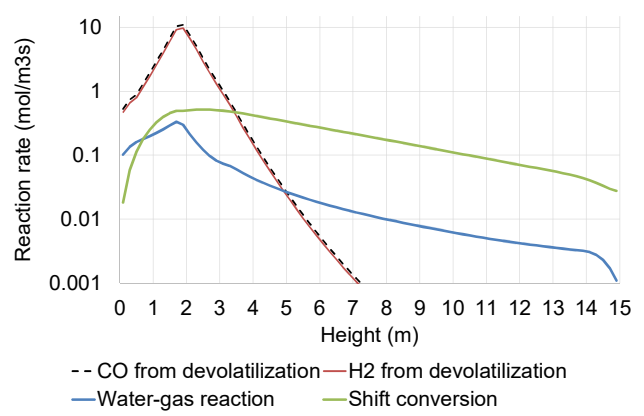

Fig. 7. Main reaction rate profiles in the centre-line of the gasifier for basic case.

Fig. 8 presents the vertical temperature profiles. The highest temperature in the gasifier is near the entry point of hot solids from the combustor. Above that, the temperature decreases due to endothermic reactions. At the upper part, the temperature is almost constant, i.e. the exothermic shift conversion is balanced by the heat loss through the walls and endothermic gasification reactions. In the combustor, the temperature is increasing as a function of height due to combustion reactions, which continue throughout the furnace with elutriative wood. The temperature difference between the outlets of combustor and gasifier was 92...103°C (lower difference with higher load). The vertical gas velocities are shown in Fig. 9. In the combustor, the average velocity increased from 3.8 to 6.8 m/s as the fuel input to combustor increased from zero to 0.15 kg/s. In the gasifier, the velocity was affected mainly by temperature and the average velocity varied from 2.5 to 3.0 m/s.
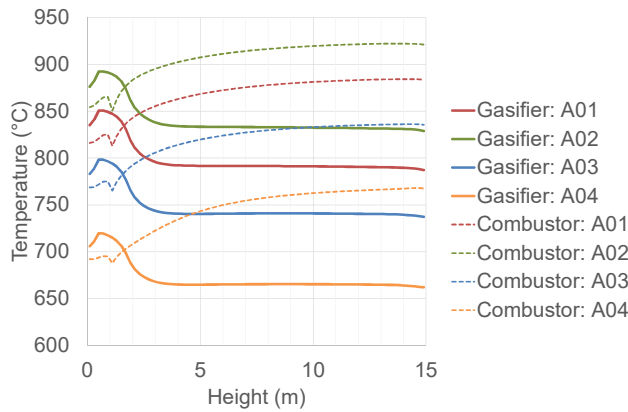

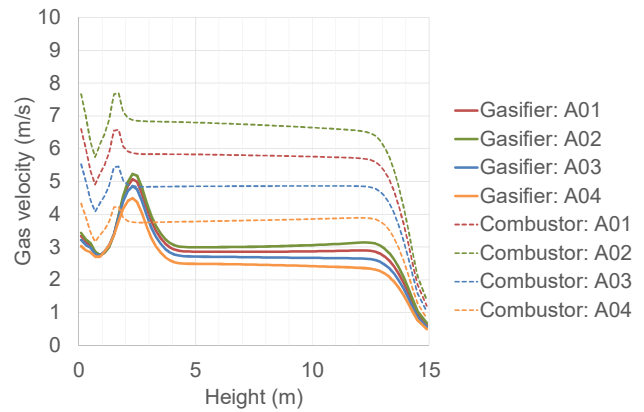Fig. 8. Temperature profiles in the centre-line of the reactors.

Fig. 9. Vertical gas velocity profiles in the centre-line of the reactors.

The gas concentration of the producer gas is presented in Fig. 10. Because the amount of fuel feed to the gasifier is constant, and thus, the amount of gases from devolatilization is not changing, the gas concentration is mostly affected by changes in the shift conversion and the water-gas reaction (Fig. 11). The water-gas reaction rate by Eq. (7) increases as a function of temperature. On the other hand, with the modelled gas compositions, a higher temperature results to smaller shift conversion as calculated by Eq. (9). A higher water-gas reaction increases the production of CO and H_2 from char. At the same time, the decreasing shift conversion reduces the conversion of CO and H_2O to CO_2 and H_2. As seen in Fig. 11, the changes in the two reactions are almost the same, but in opposite direction. As a consequence, the H_2 concentration is not much changing as a function of temperature, because the two reactions are compensating each other. The CO_2 level

is decreasing due to decreasing shift conversion as the temperature increases. The CO level is increasing due to increasing water-gas reaction and decreasing shift conversion.

The modelled case is a conceptual study, thus, proper measurement data for validating the model does not exist. However, in Fig. 10, the model results are compared with measurements from literature to evaluate the observed trends of the effect of temperature on gas composition. The data by Hafner et al. [36] present the measurements, which were carried out in a 20 kW$_{th}$ DFB test facility at the University of Stuttgart at temperature level above the calcination temperature, i.e. when the calcination/carbonation reactions were not affecting the gas composition. The data by Hofbauer et al. show the trends of the measurements in a 100 kW$_{th}$ FICFB pilot at the University of Vienna [70]. In both cases, wood pellets were used as fuel.

In the measurements, the H$_2$ content is increasing as the temperature increases. In the model, the H$_2$ content was almost constant due to opposite changes in the affecting reactions: water-gas reaction and shift conversion (Fig. 11). In the model, the generation of H$_2$ from the devolatilization should probably be smaller at the lower temperature. This finding is supported by bench scale tests [71]. The modelled level of H$_2$ (44...45 %-vol,dry) is between the measured values (35 – 50 %-vol,dry). The considerably higher proportion of H$_2$ in the measurements by Hafner et al. might be due to catalytic effects of the limestone, which was used as bed material.

The trends of CO and CO$_2$ are similar in the measurements and the model: CO increases and CO$_2$ decreases a a function of temperature. Based on the model, this effect can be due to increasing water-gas reaction and decreasing shift conversion (Fig. 11). The measured CO levels are higher and the CO$_2$ levels lower than in the model. Probably the CO/CO$_2$-ratio of the devolatilized gases should have been higher in the model.

The contents of hydrocarbons (CH$_4$ and C$_2$H$_4$) are not much affected by the temperature in the model. This is similar in the measurements as well. The modelled level of CH$_4$ is close to measurements by Hofbauer et al. [70]. According to Hofbauer et al., the rest of the hydrocarbons were mostly ethene (C$_2$H$_4$), thus, it is a reasonable selection in the model to represent the higher hydrocarbons. The amount of modelled C$_2$H$_4$ was slightly higher than in the measurements.
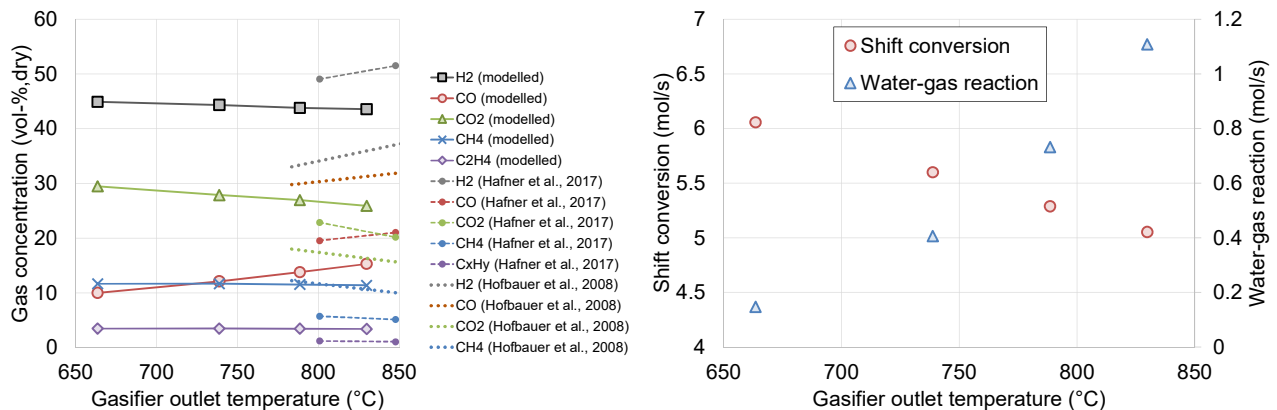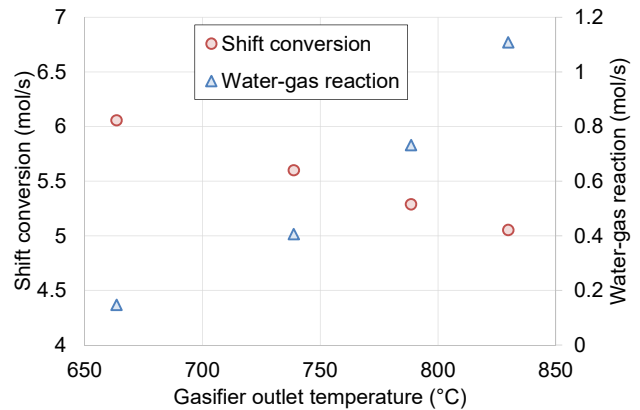

Fig. 10. Modelled producer gas concentration compared with measurements by Hafner et al. [36] and Hofbauer et al. [70].

Fig. 11. Shift conversion and water-gas reaction.

Comparing with the incoming steam, the consumption of H$_2$O in different reactions is relatively small. The sum of shift conversion and water-gas reaction, which both consume H$_2$O, is about constant in all cases (6.0...6.2 mol/s). As the steam flow to gasifier was constant (0.45 kg/s = 25.0 mol/s) and the biomass feed to gasifier was constant (0.9 kg/s fuel feed generating 12.5 mol/s H$_2$O from moisture), the total H$_2$O conversion is about 16% in all cases, i.e. about 84% of steam is leaving the gasifier unreacted. The modelled low conversion ratios of steam match well with the experimental data in literature [1,70].

Fig. 12 presents the lower heat value of producer gas and the cold gas efficiency and Fig. 13 presents the mass flow of char from gasifier and combustor in different cases.
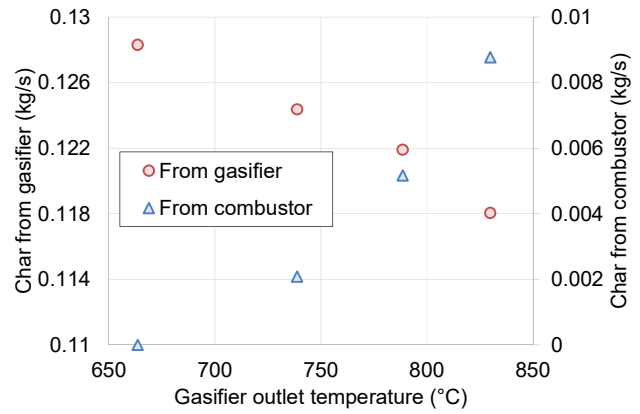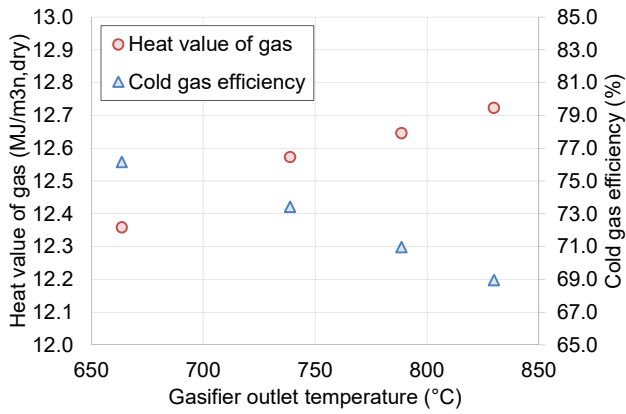
Fig. 12. Heat value of producer gas and cold gas efficiency.

Fig. 13. Char flow rate from gasifier and combustor.

The cold gas efficiency (sometimes called chemical efficiency) is defined as the chemical heat of the produced producer gas divided by the total fuel power fed to gasifier and combustor:

$$\eta_{CG} = \frac{q_{v,gas} Q_{gas,LHV}}{\sum q_{m,fuel} Q_{fuel,LHV}} \tag{10}$$

In direct air- or oxygen-blown gasification, the higher gasification temperature leads to lower heat value of gas. This is because the higher temperature is achieved by increasing the amount of oxygen, which increases the oxidation reactions and reduces the share of combustible gases. In indirect steam gasification, the higher temperature is achieved by increasing the fuel input to combustor. This increases the gas yield from gasification of char. Consequently, the heat value of gas is higher with a higher gasification temperature. As noted earlier, most of the producer gas originates from the devolatilization. Consequently, the increase in the gas yield is relatively small and thus, the increment in the chemical heat of producer gas is smaller than the increment of the fuel power. Consequently, the cold gas efficiency decreases with higher fuel input to combustor.

The unreacted char from gasifier is transferred to combustor with the other circulating solids. Based on these calculations, the amount of char from gasifier, which is burned in combustor is enough to sustain the gasification process. As the temperature increases, the water-gas reaction is enhanced and the char flow from gasifier decreases (Fig. 13). The char flow from combustor is considerably smaller as most of the char is burned. Increasing the temperature by higher fuel input to combustor increases the superficial gas velocity and decreases the residence time of char in the combustor. Consequently, this leads to higher char flow rate at the outlet of the combustor. At minimum temperature, when no fuel is fed to combustor, the char flow rate is almost zero, i.e. all the char from gasifier is burned in the combustor.

The modelled case does not represent any existing facility, thus, direct validation data is not available. Table 3 compares the main modelled parameters with the measurement data of indirect steam gasification from literature. The data of Technical University of Vienna (TUW) is from a 120 kW_{th} pilot plant using wood pellets [34]. The data of Güssing is from a 8 MW_{th} biomass gasifier [35]. In both cases, the gasifier operated in BFB mode. There are some differences in the modelled producer gas composition compared with measurements: higher H_2, lower CO, higher CO_2, and higher H_2O. The shares of hydrocarbons match the measurements well considering that the model does not simulate the heavier hydrocarbons (C_2H_6, C_3H_8), i.e. the modelled C_2H_4 can be interpreted to represent them as well. The differences can be partly due to different process conditions, e.g. higher fuel moisture, longer residence time, and BFB vs CFB mode. Other explanations are that the submodel for devolatilization predicted a too small CO/CO_2-ratio and/or the shift conversion rate was too high.

Based on the effect of temperature on different gas components, the generation of H_2 from the devolatilization should be lower at the lower temperatures. A revision of the devolatilization model is definitely needed to improve the prediction capability of the model. Moreover, good measurement data of a large scale

unit would be required for model validation. Profile measurements of gas concentrations and temperatures in different regions of the gasifier would be desired, however, achieving them from industrial units is difficult. Besides updating of the devolatilization model, various other model parameters can be later adjusted when validation data is available. For now, this study showed the feasibility of the model approach for large scale modelling of a DFB gasifier and how the model can help to analyse the effects of changing process conditions on the gasifier performance.

Table 3. Modelled process data compared with measurement data from literature.

Parameter	Units	TUW	Güssing	Case A01	Case A02	Case A03	Case A04
Gasification temperature	(°C)	841	800...900	789	830	739	664
Combustion temperature	(°C)	920	n.a.	884	922	836	767
Steam/fuel ratio	(-)	0.63	0.6...0.7	0.5	0.5	0.5	0.5
H_2	(vol-%,dry)	39.1	38...40	43.8	43.5	44.3	44.9
CO	(vol-%,dry)	29.1	24...26	13.8	15.3	12.1	10.0
CO_2	(vol-%,dry)	17.5	20...22	27.0	25.9	27.9	29.5
CH_4	(vol-%,dry)	11.4	10...11	11.5	11.4	11.7	11.7
C_2H_4	(vol-%,dry)	2.0	2.0...2.5	3.5	3.4	3.5	3.5
$C_2H_6 + C_3H_8$	(vol-%,dry)	0.9	0.5...1.0	n.m.	n.m.	n.m.	n.m.
H_2O	(vol-%,wet)	33.2	30...45	47.7	47.3	48.1	47.9
LHV	(MJ/m^3n,dry)	13.7	12.9...13.6	12.65	12.72	12.57	12.36

5.   Conclusions

The presented semi-empirical modelling method is an efficient tool for simulating indirect steam gasification in coupled gasifier/combustor CFB reactors. The model helps to analyse the different phenomena occurring in the reactors and to study the effects of process parameters on producer gas composition and cold gas efficiency. Based on the simulations, the process can be operated without additional fuel to combustor. Increasing the fuel input to combustor increases the gasification temperature, which increases the heat value of the producer gas slightly, but reduces the cold gas efficiency of the system.

The modelled case was a conceptual study and measurement data for validation did not exist. Based on comparison with the measurements in literature, the model could simulate many of the observed trends correctly, e.g. the effect of temperature on CO and CO_2 concentrations and the low conversion ratio of steam in indirect steam gasification. However, the devolatilization model should be revised so that it could better simulate the distribution of the generated gas components. Moreover, the model should be validated by full scale measurements. This will be the aim of the future studies.

In the modelled cases, the limestone feed was small and the calcination and carbonation reactions did not contribute much to the producer gas composition. In future, the model concept can be applied to study sorption enhanced gasification, in which the CO_2 can be decreased in the gasifier by carbonation of lime.

Nomenclature

a	coefficient, 1/s		T	temperature, K
b	model parameter, -		w	weight fraction, -
c	model parameter, -		ε	volume fraction, -
C	molar concentration, mol/m^3		η_{CG}	cold gas efficiency, -
d_p	particle size, m		ρ	density, kg/m^3
d_{ref}	reference size, m			
E	activation energy, J/mol		Subscripts	
$q_{m,fuel}$	fuel mass flow rate, kg/s		$boud$	Boudouard reaction
$q_{v,gas}$	producer gas flow rate, m^{3}n/s		$char$	char (fixed carbon)
$Q_{fuel,LHV}$	lower heat value of fuel, MJ/kg		i	particle size group
$Q_{gas,LHV}$	lower heat value of gas, MJ/m^{3}n		$shift$	shift conversion
r'''	reaction source term, mol/m^{3}s		vol	volatiles (in solid form)
R'''	reaction source term, kg/m^{3}s		wat	moisture
R	universal gas constant, J/(mol K)		$watg$	water-gas reaction

Acknowledgement

References

[1] J. Corella, J.M. Toledo, G. Molina, A review on dual fluidized-bed biomass gasifiers, Ind. Eng. Chem. Res. 46 (2007) 6831–6839. doi:10.1021/ie0705507.

[2] M. Hasegawa, J. Fukuda, D. Kunii, Gasification of solid waste in a fluidized bed reactor with circulating sand, Conserv. Recycl. 3 (1979) 143–153. doi:10.1016/0361-3658(79)90004-3.

[3] R. Bailie, Production of high energy fuel gas from municipal wastes, United States Patent 3,853,498, 1974.

[4] D. Kunii, T. Kunugi, Process and apparatus for thermal cracking of hydrocarbons, United States Patent 3,708,552, 1973.

[5] M. Igarashi, Y. Hayafune, R. Sugamiya, Y. Nakagawa, K. Makishima, Pyrolysis of Municipal Solid Waste in Japan, J. Energy Resour. Technol. 106 (1984) 377–382. doi:10.1115/1.3231068.

[6] C.H. Liao, M. Summers, R. Seiser, R. Cattolica, R. Herz, Simulation of a pilot-scale dual-fluidized-bed gasifier for biomass, in: Environ. Prog. Sustain. Energy, 2014: pp. 732–736. doi:10.1002/ep.11945.

[7] M.A. Paisley, J.M. Irving, R.P. Overend, A promising power option-The FERCO Silvagas^{TM} biomass gasification process-operating experience at the Burlington gasifier, in: Proc. ASME Turbo Expo, 2001. doi:10.1115/2001-GT-0370.

[8] E4Tech, Review of Technologies for Gasification of Biomass and Wastes, 2009. http://www.e4tech.com/wp-content/uploads/2016/01/gasification2009.pdf.

[9] J. Hansson, A. Leveau, C. Hulteberg, Biomass gasifier database for computer simulation purposes, 2011. http://www.sgc.se/ckfinder/userfiles/files/SGC234.pdf.

[10] J. Lane, Rentech to close Colorado demo unit, drop advanced biofuels R&D activities, Biofuels Dig. (2013) 1–2. http://www.biofuelsdigest.com/bdigest/2013/03/01/rentech-to-close-colorado-demo-unit-drop-advanced-biofuels-rd-activities/.

[11] H. Hofbauer, G. Veronik, T. Fleck, R. Rauch, H. Mackinger, E. Fercher, The FICFB gasification process, in: A.V. Bridgwater, D. Boocock (Eds.), Dev. Thermochem. Biomass Convers., Blackie Academic & Professional, Glasgow, 1997: pp. 1016–1025. doi:10.1007/978-94-009-1559-6.

[12] H. Hofbauer, R. Rauch, K. Bosch, R. Koch, C. Aichernig, Biomass CHP Plant Güssing - A Success Story, in: A.V. Bridgwater (Ed.), Pyrolysis Gasif. Biomass Waste, CPL Press, Newsbury, 2003: pp. 371–383. http://members.aon.at/biomasse/strassbourg.pdf.

[13] West Biofuels, Projects, (2017). http://www.westbiofuels.com/projects?filter=ficfb# (accessed November 2, 2017).

[14] Göteborg Energi, GoBiGas - anläggningen, (2017). https://gobigas.goteborgenergi.se/Svensk_version/Anlaggningen (accessed November 2, 2017).

[15] C.M. Van Der Meijden, H. Veringa, B.J. Vreugdenhil, a. Van Der Drift, R.W.R. Zwart, R. Smit, Production of bio-methane from woody biomass, in: World Gas Conf., 2009: pp. 3965–3971.

[16] Royal Dahlman, MILENA Gasifier under Construction | Royal Dahlman, (2017). http://www.royaldahlman.com/renewable/news/commercial-milena-gasifier-under-construction/ (accessed November 2, 2017).

[17] C.M. Van Der Meijden, B.J. Vreugdenhil, G.A. Almansa, Production of bio-methane from woody biomass using the MILENA gasification technology, in: Int. Bioenergy Exhib. Asian Bioenergy Conf., 2015: pp. 61–67. doi:10.5071/IBSCE2015-3BO.1.2.

[18] C.M. van der Meijden, L.P.L.M. Rabou, B.J. Vreugdenhil, R. Smit, Large Scale Production of Bio Methane from Wood, in: Int. Gas Union Res. Conf. IGRC, 2011.

[19] D. Sutton, B. Kelleher, J.R.H. Ross, Review of literature on catalysts for biomass gasification, Fuel Process. Technol. 73 (2001) 155–173. doi:10.1016/S0378-3820(01)00208-9.

[20] Y. Shen, K. Yoshikawa, Recent progresses in catalytic tar elimination during biomass gasification or pyrolysis - A review, Renew. Sustain. Energy Rev. 21 (2013) 371–392. doi:10.1016/j.rser.2012.12.062.

[21] H. Hofbauer, R. Rauch, G. Loeffler, S. Kaiser, E. Fercher, H. Tremmel, Six years experience with the FICFB-gasification process, 12th Eur. Conf. Technol. Exhib. Biomass Energy, Ind. Clim. Prot. (2002) 982–985. http://members.aon.at/biomasse/six_years.pdf.

[22] C. Pfeifer, R. Rauch, H. Hofbauer, In-Bed Catalytic Tar Reduction in a Dual Fluidized Bed Biomass Steam Gasifier, Ind. Eng. Chem. Res. 43 (2004) 1634–1640. doi:10.1021/ie030742b.

[23] S. Rapagnà, N. Jand, A. Kiennemann, P.U. Foscolo, Steam-gasification of biomass in a fluidised-bed of olivine particles, Biomass and Bioenergy. 19 (2000) 187–197. doi:10.1016/S0961-9534(00)00031-3.

[24] F. Miccio, B. Piriou, G. Ruoppolo, R. Chirone, Biomass gasification in a catalytic fluidized reactor with beds of different materials, Chem. Eng. J. 154 (2009) 369–374. doi:10.1016/j.cej.2009.04.002.

[25] T. Berdugo Vilches, J. Marinkovic, M. Seemann, H. Thunman, Comparing Active Bed Materials in a Dual Fluidized Bed Biomass Gasifier: Olivine, Bauxite, Quartz-Sand, and Ilmenite, Energy and Fuels. 30 (2016) 4848–4857. doi:10.1021/acs.energyfuels.6b00327.

[26] A. Chiodini, L. Bua, L. Carnelli, R. Zwart, B. Vreugdenhil, M. Vocciante, Enhancements in Biomass-to-Liquid processes: Gasification aiming at high hydrogen/carbon monoxide ratios for direct Fischer-Tropsch synthesis applications, Biomass and Bioenergy. 106 (2017) 104–114. doi:10.1016/j.biombioe.2017.08.022.

[27] G.P. Curran, C.H. Rice, E. Gorin, Carbon dioxide acceptor gasification process, Prepr. Pap. Am. Chem. Soc. Div. Fuel Chem. 8 (1964) 128–146. http://pubs.acs.org/doi/abs/10.1021/ba-1967-0069.ch010.

[28] C. Pfeifer, B. Puchner, H. Hofbauer, In-situ CO2-absorption in a dual fluidized bed biomass steam gasifier to produce a hydrogen rich syngas, Int. J. Chem. React. Eng. 5 (2007) A9. doi:10.2202/1542-6580.1395.

[29] N.H. Florin, A.T. Harris, Enhanced hydrogen production from biomass with in situ carbon dioxide capture using calcium oxide sorbents, Chem. Eng. Sci. 63 (2008) 287–316. doi:10.1016/j.ces.2007.09.011.

[30] G. Soukup, C. Pfeifer, A. Kreuzeder, H. Hofbauer, In situ CO2 capture in a dual fluidized bed biomass steam gasifier - Bed material and fuel variation, Chem. Eng. Technol. 32 (2009) 348–354. doi:10.1002/ceat.200800559.

[31] I. Martínez, M.C. Romano, Flexible sorption enhanced gasification (SEG) of biomass for the production of synthetic natural gas (SNG) and liquid biofuels: Process assessment of stand-alone and power-to-gas plant schemes for SNG production, Energy. 113 (2016) 615–630. doi:10.1016/j.energy.2016.07.026.

[32] J. Udomsirichakorn, P.A. Salam, Review of hydrogen-enriched gas production from steam gasification of biomass: The prospect of CaO-based chemical looping gasification, Renew. Sustain. Energy Rev. 30 (2014) 565–579. doi:10.1016/j.rser.2013.10.013.

[33] S. Koppatz, C. Pfeifer, R. Rauch, H. Hofbauer, T. Marquard-Moellenstedt, M. Specht, H2 rich product gas by steam gasification of biomass with in situ CO2 absorption in a dual fluidized bed system of 8 MW fuel input, Fuel Process. Technol. 90 (2009) 914–921. doi:10.1016/j.fuproc.2009.03.016.

[34] C. Pfeifer, B. Puchner, H. Hofbauer, Comparison of dual fluidized bed steam gasification of biomass with and without selective transport of CO2, Chem. Eng. Sci. 64 (2009) 5073–5083. doi:10.1016/j.ces.2009.08.014.

[35] M. Specht, Biomass fluidised bed gasification with in-situ hot gas cleaning. AER-Gas II, publishable final activity report, 2009. http://cordis.europa.eu/documents/documentlibrary/126625711EN6.pdf.

[36] S. Hafner, N. Armburst, R. Spörl, G. Scheffknecht, Production of tailored syngas for dimethyl ether synthesis by sorption enhanced gasification, in: W. Nowak, M. Sciazko, P. Mirek (Eds.), 12th Int. Conf. Fluid. Bed Technol., Printing House of the Redemptorists, Tuchow, 2017: pp. 781–786.

[37] T.A. Semelsberger, R.L. Borup, H.L. Greene, Dimethyl ether (DME) as an alternative fuel, J. Power Sources. 156 (2006) 497–511. doi:10.1016/j.jpowsour.2005.05.082.

[38] W. Ying, L. Genbao, Z. Wei, Z. Longbao, Study on the application of DME/diesel blends in a diesel engine, Fuel Process. Technol. 89 (2008) 1272–1280. doi:10.1016/j.fuproc.2008.05.023.

[39] G. Schuster, G. Löffler, K. Weigl, H. Hofbauer, Biomass steam gasification--an extensive parametric modeling study., Bioresour. Technol. 77 (2001) 71–79. doi:10.1016/S0960-8524(00)00115-2.

[40] B. Rehling, H. Hofbauer, R. Rauch, C. Aichernig, BioSNG-process simulation and comparison with first results from a 1-MW demonstration plant, Biomass Convers. Biorefinery. 1 (2011) 111–119. doi:10.1007/s13399-011-0013-3.

[41] S. Kaiser, K. Weigl, G. Schuster, H. Tremmel, A. Friedl, H. Hofbauer, Simulation and optimization of a biomass gasification process, in: S. Kyrisits (Ed.), Proc. First World Conf. Biomass Energy Ind., James&James, London, 2000: p. 1922–1925.

[42] L. Abdelouahed, O. Authier, G. Mauviel, J.P. Corriou, G. Verdier, A. Dufour, Detailed modeling of biomass gasification in dual fluidized bed reactors under Aspen Plus, Energy and Fuels. 26 (2012) 3840–3855. doi:10.1021/ef300411k.

[43] M.B. Nikoo, N. Mahinpey, Simulation of biomass gasification in fluidized bed reactor using ASPEN PLUS, Biomass and Bioenergy. 32 (2008) 1245–1254. doi:10.1016/j.biombioe.2008.02.020.

[44] A. Alamia, H. Thunman, M. Seemann, Process Simulation of Dual Fluidized Bed Gasifiers Using Experimental Data, Energy and Fuels. 30 (2016) 4017–4033. doi:10.1021/acs.energyfuels.6b00122.

[45] M. Gassner, F. Maréchal, Thermo-economic process model for thermochemical production of Synthetic Natural Gas (SNG) from lignocellulosic biomass, Biomass and Bioenergy. 33 (2009) 1587–1604. doi:10.1016/j.biombioe.2009.08.004.

[46] B. Guo, D. Li, C. Cheng, Z. Lü, Y. Shen, Simulation of biomass gasification with a hybrid neural network model, Bioresour. Technol. 76 (2001) 77–83. doi:10.1016/S0960-8524(00)00106-1.

[47] J. Corella, A. Sanz, Modeling circulating fluidized bed biomass gasifiers . A pseudo-rigorous model for stationary state, Fuel Process. Technol. 86 (2005) 1021–1053. doi:10.1016/j.fuproc.2004.11.013.

[48] P. Kaushal, J. Abedi, N. Mahinpey, A comprehensive mathematical model for biomass gasification in a bubbling fluidized bed reactor, Fuel. 89 (2010) 3650–3661. doi:10.1016/j.fuel.2010.07.036.

[49] H. Noubli, S. Valin, B. Spindler, M. Hemati, Development of a modelling tool representing biomass gasification step in a dual fluidized bed, Can. J. Chem. Eng. 93 (2015) 340–347. doi:10.1002/cjce.22124.

[50] I. Petersen, J. Werther, Experimental investigation and modeling of gasification of sewage sludge in the circulating fluidized bed, Chem. Eng. Process. Process Intensif. 44 (2005) 717–736. doi:10.1016/j.cep.2004.09.001.

[51] I. Petersen, J. Werther, Three-dimensional modeling of a circulating fluidized bed gasifier for sewage sludge, Chem. Eng. Sci. 60 (2005) 4469–4484. doi:10.1016/j.ces.2005.02.058.

[52] K. Myöhänen, T. Hyppänen, A three-dimensional model frame for modelling combustion and gasification in circulating fluidized bed furnaces, Int. J. Chem. React. Eng. 9 (2011) A25.

[53] M. Koski, J. Ritvanen, K. Myöhänen, T. Hyppänen, J. Palonen, K. Häkkinen, S. Kokki, Three-dimensional modelling of steam-oxygen gasification in a circulating fluidized bed, in: U. Arena, R. Chirone, M. Miccio, P. Salatino (Eds.), Proc. 21st Int. Conf. Fluid. Bed Combust., EnzoAlbanoEditore, Naples, 2012: pp. 883–890.

[54] M.J. Andrews, P.J. O'Rourke, The multiphase particle-in-cell (MP-PIC) method for dense particulate flows, Int. J. Multiph. Flow. 22 (1996) 379–402. doi:10.1016/0301-9322(95)00072-0.

[55] N.A. Patankar, D.D. Joseph, Modeling and numerical simulation of particulate flows by the Eulerian-Lagrangian approach, Int. J. Multiph. Flow. 27 (2001) 1659–1684. doi:10.1016/S0301-9322(01)00021-0.

[56] H. Liu, R.J. Cattolica, R. Seiser, C. hsien Liao, Three-dimensional full-loop simulation of a dual fluidized-bed biomass gasifier, Appl. Energy. 160 (2015) 489–501. doi:10.1016/j.apenergy.2015.09.065.

[57] S. Kraft, F. Kirnbauer, H. Hofbauer, CPFD simulations of an industrial-sized dual fluidized bed steam

gasification system of biomass with 8 MW fuel input, Appl. Energy. 190 (2017) 408–420. doi:10.1016/j.apenergy.2016.12.113.

[58] L. Yan, C.J. Lim, G. Yue, B. He, J.R. Grace, Simulation of biomass-steam gasification in fluidized bed reactors: Model setup, comparisons and preliminary predictions, Bioresour. Technol. 221 (2016) 625–635. doi:10.1016/j.biortech.2016.09.089.

[59] T. Hyppänen, Y.Y. Lee, A. Rainio, Three-dimensional model for circulating fluidized bed boilers, in: E.J. Anthony (Ed.), Proc. Int. Conf. Fluid. Bed Combust., ASME, New York, 1991: pp. 439–448.

[60] M. Lyytikäinen, A. Kettunen, K. Myöhänen, T. Hyppänen, Utilization of a three dimensional model in designing and tuning of a large scale CFB boiler, in: J. Li, F. Wei, X. Bao, W. Wang (Eds.), Proc. 11th Int. Conf. Fluid. Bed Technol., Chemical Industry Press, Beijing, 2014: pp. 823–828.

[61] S. Shah, M. Klajny, K. Myöhänen, T. Hyppänen, Improvement of CFD methods for modeling full scale circulating fluidized bed combustion systems, in: Proc. 20th Int. Conf. Fluid. Bed Combust., 2009.

[62] M. Nikku, K. Myöhänen, J. Ritvanen, T. Hyppänen, Three-dimensional modeling of fuel flow with a holistic circulating fluidized bed furnace model, Chem. Eng. Sci. 117 (2014) 352–363. doi:10.1016/j.ces.2014.06.038.

[63] R.H. Perry, D.W. Green, J.O. Maloney, eds., Energy Resources, Conversion, and Utilization, in: Perry's Chem. Eng. Handb., McGraw-Hill, New York, 1997.

[64] K. Luecke, E. Hartge, J. Werther, A 3D Model of Combustion in Large-Scale Circulating Fluidized Bed Boilers A 3D Model of Combustion in Large-Scale Circulating Fluidized Bed Boilers, Int. J. Chem. React. Eng. 2 (2004) A11.

[65] R. Wischnewski, L. Ratschow, E.U. Hartge, J. Werther, Reactive gas-solids flows in large volumes-3D modeling of industrial circulating fluidized bed combustors, Particuology. 8 (2010) 67–77. doi:10.1016/j.partic.2009.08.001.

[66] G. Migliavacca, E. Parodi, L. Bonfanti, T. Faravelli, S. Pierucci, E. Ranzi, A general mathematical model of solid fuels pyrolysis, Energy. 30 (2005) 1453–1468. doi:10.1016/j.energy.2004.02.011.

[67] J.J. Saastamoinen, Simplified model for calculation of devolatilization in fluidized beds, Fuel. 85 (2006) 2388–2395. doi:10.1016/j.fuel.2006.04.019.

[68] V. Biba, J. Macák, E. Klose, J. Malecha, Mathematical Model for the Gasification of Coal under Pressure, Ind. Eng. Chem. Process Des. Dev. 17 (1978) 92–98. doi:10.1021/i260065a017.

[69] H. Yoon, J. Wei, M.M. Denn, A model for moving-bed coal gasification reactors, AIChE J. 24 (1978) 885–903. doi:10.1002/aic.690240515.

[70] H. Hofbauer, R. Rauch, Stoichiometric Water Consumption of Steam Gasification by the FICFB-Gasification Process, in: A.V. Bridgwater (Ed.), Prog. Thermochem. Biomass Convers., Wiley, 2008: pp. 199–208. doi:10.1002/9780470694954.ch14.

[71] L. Fagbemi, L. Khezami, R. Capart, Pyrolysis products from different biomasses, Appl. Energy. 69 (2001) 293–306. doi:10.1016/S0306-2619(01)00013-7.